Technical Notes

TECHNICAL NOTES are short manuscripts describing new developments or important results of a preliminary nature. These Notes cannot exceed 6 manuscript pages and 3 figures; a page of text may be substituted for a figure and vice versa. After informal review by the editors, they may be published within a few months of the date of receipt. Style requirements are the same as for regular contributions (see inside back cover).

J 80-022

Pulsed Raman Measurements in a Stratified Charge Engine

J. Ray Smith*
Sandia Laboratories, Livermore, Calif.

0004
0023

Introduction

ATTEMPTS to satisfy emissions and fuel economy regulations have been hindered by the fact that current analytical models of combustion chamber processes cannot describe the turbulent gas properties within reciprocating internal combustion engines. The motivation for measuring temporal and spatial variations of gas properties is to provide insight into the detailed processes that occur and to develop a data base for analytical model verification. The feasibility of utilizing time-averaged spontaneous Raman scattering in a combusting engine to yield spatial information was first demonstrated in 1976.[1] Recently, a stratified charge engine with good optical access was developed, and its fuel-air distributions were measured by time-averaged Raman spectroscopy. Its precombustion velocity and turbulence fields were measured by laser Doppler velocimetry and its performance and emissions were obtained by conventional methods.[2] The same engine design was used in this study.

This Note discusses a time-resolved technique for measuring both mean and fluctuating components of nitrogen number density in a combusting engine and some typical results. Some of the difficulties and their practical solutions are also discussed.

Discussion

The engine used has been designed to simplify the fluid mechanics for modeling purposes. The intake and exhaust valves, fuel injector, spark plug, and laser input/output windows are located in the cylinder sidewalls in the clearance volume above the piston. The head contains a 70-mm-diam clear aperture window. The laser beam is passed through the small windows and scattered light is collected at right angles to the beam through the large window in the top of the engine. The intake valve is shrouded to provide swirl to the airflow. Propane at 3.35 MPa (485 psi) and 100°C is injected radially toward the center of the bore. The overall equivalence ratio of the data presented is 0.7 (i.e., 70% of the fuel required to give a stoichiometric fuel-air ratio) and the engine speed is 900 rpm.

The experimental arrangement is shown in Fig. 1. A shaft encoder is used to time the laser firing to the required crank angle. The Raman scattered light is imaged into the slit of a 3/4 m, single spectrometer and detected by a cooled RCA C31034A photomultiplier tube (PMT). Only the first six stages of the PMT are used to maintain linearity with high dynamic range. The PMT output charge is integrated by a preamplifier, pulse shaped by a spectroscopy amplifier, digitized, and collected by a minicomputer. The Raman signal is normalized by the laser pulse energy, and by accounting for the amplifier gain, the number of photoelectrons is recorded. One thousand measurements are taken during successive engine cycles at each crank angle selected. Checks for possible sensitivity changes (due to window transmission) are made during the course of the data acquisition, by repeating measurements at a given crank angle. The maximum sensitivity variation observed over a 1-h period of lean engine operation has been 2.4% change in the mean value.

The first major problem that must be solved in making nitrogen number density measurements in a turbulent flow was pointed out by Setchell[3] to be the coupling of the temperature into the Raman-scattered intensity. Because the transition probability is greater for the upper vibrational states than for the lower states, the integrated Raman-scattered intensity is not a unique function of number density. However, a theoretical analysis of the Stokes vibrational Raman spectrum of nitrogen has led to a method of making nitrogen measurements that are essentially independent of temperature. A variety of spectrometer slit convolutions with nitrogen Stokes spectra at various slit center wavelength positions were studied to determine their influence on the integrated Stokes Raman intensity vs temperature. The problem reduces to selection of a center position of the bandpass, which balances the increase in Raman scattering from the higher vibrational states against the decrease in population of the ground state as the temperature rises. For a frequency doubled YAG laser (532.1 nm) it was found that by using a 1×5 nm trapazoidal slit function centered at 607.2 nm, the Stokes intensity varies by only $\pm 2\%$ from 300 to nearly 2000 K.

Sub-microsecond time resolution is achieved by using a Q-switched laser having a pulse width of 10^{-2} μs. Although this laser was capable of producing in excess of 250 mJ per pulse, only 50 mJ were used in the experiment. Above this energy level, the chances of window damage greatly increased. All of the data presented here were gathered with less than 20 MW/cm^2 power densities in the input/output windows. The high power density of the laser also causes gas breakdown[4] at the focal point unless large astigmatism is introduced by tilting the focusing lens relative to the beam axis. This method was used to give a scattering volume of 0.5 mm diameter by 1.25 mm in length. The length dimension being determined by the 4-power magnification of the collection optics and the spectrometer entrance slit height of 5 mm. A check of the linearity of the Raman signal vs both nitrogen density and laser beam energy input well beyond the ranges of the experiment was within 2% agreement.

The Raman scattering process is very weak and the number of photoelectrons produced per pulse will obey Poisson statistics. However, if more than 100 photoelectrons are produced in each event, the uncertainty (one standard deviation) in the actual number of photoelectrons, N, may be approximated by:

$$\sigma_p = \sqrt{N} \tag{1}$$

Since nitrogen number density fluctuations, σ_f, are not related to the photoelectron fluctuations, σ_p, they will combine randomly to give a signal fluctuation of:

$$\sigma_s = \sqrt{\sigma_f^2 + \sigma_p^2} \tag{2}$$

Therefore, the actual fluctuations may be assessed by taking a sufficiently large sample of measurements to compute σ_s and

Received June 26, 1979. This paper is declared a work of the U.S. Government and therefore is in the public domain.

Index categories: Combustion Efficiency; Reciprocating Machinery.

*Member of Technical Staff, Combustion Applications Division.

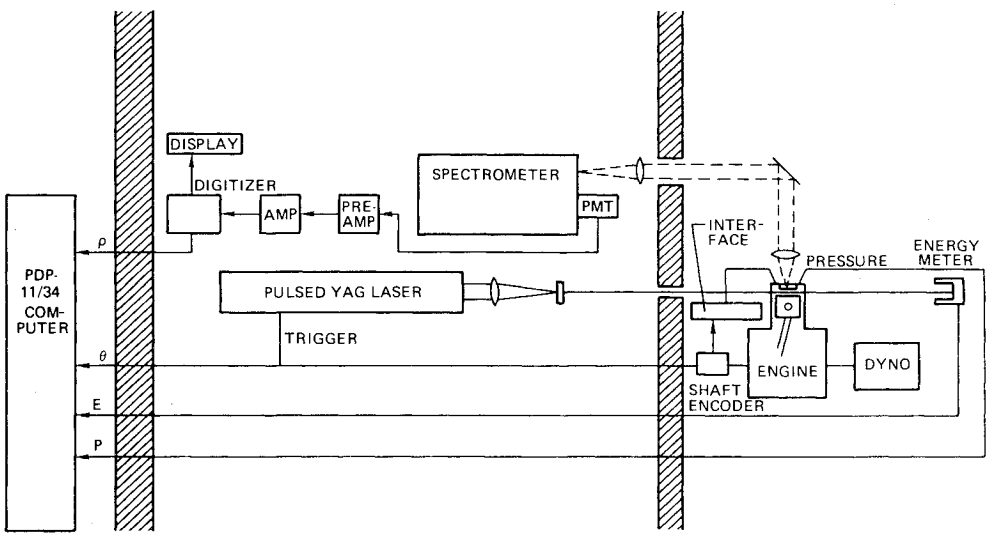

Fig. 1 Experimental arrangements of time-resolved Raman experiment.

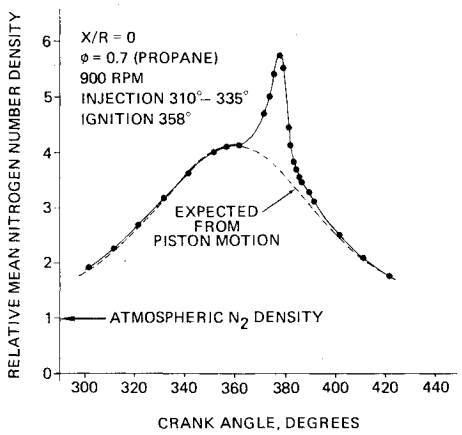

Fig. 2 Relative mean nitrogen number density vs crank angle.

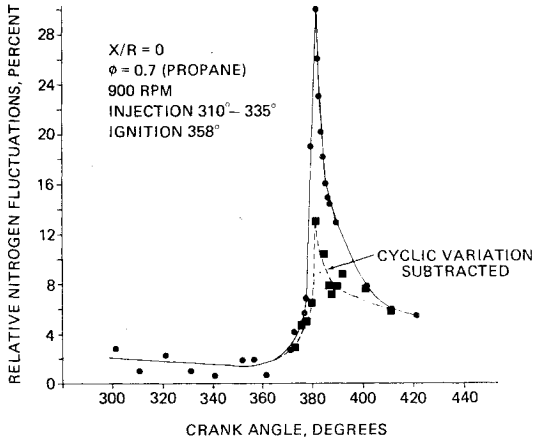

Fig. 3 One standard deviation of fluctuations in nitrogen number density.

using the mean N value of the signal to compute σ_p. This technique works well provided the actual fluctuations are at least half the size of the Poisson statistical fluctuations. Below this level, the σ_p uncertainty begins to dominate the computed σ_f value. In this experiment, 200-800 photoelectrons were collected from each laser pulse, which gives Poisson statistical uncertainties from 7 to 3.4%, respectively.

The mean values of the relative nitrogen number density vs crank angle at the center of the combustion chamber are shown in Fig. 2. Also shown for comparison is the nitrogen density expected from piston motion (dashed line). The density is relative to the nitrogen density at atmosphere pressure. Ignition occurs at 358 deg crank angle and the flame arrives at the scattering volume at about 382 deg. One observes the compression of the unburned gases ahead of the flame front after ignition. As will be shown later, the maximum number density values are reduced due to cyclic variation of the flame front arrival time at the scattering volume.

The one standard deviation fluctuations in nitrogen number density vs crank angle are the solid curves shown in Fig. 3. Prior to ignition, the fluctuation level is quite low. Fluctuations peak at flame arrival near 382 deg and fall slowly in the postflame gases. The large peak value is due to the random variations in the arrival time of the flame front, since some measurements are made just ahead of the flame front where high densities prevail, and other measurements are made just behind the flame front where the high temperatures make the densities low. The dashed curve in Fig. 3 is an attempt to remove this cyclic variation effect by using the most

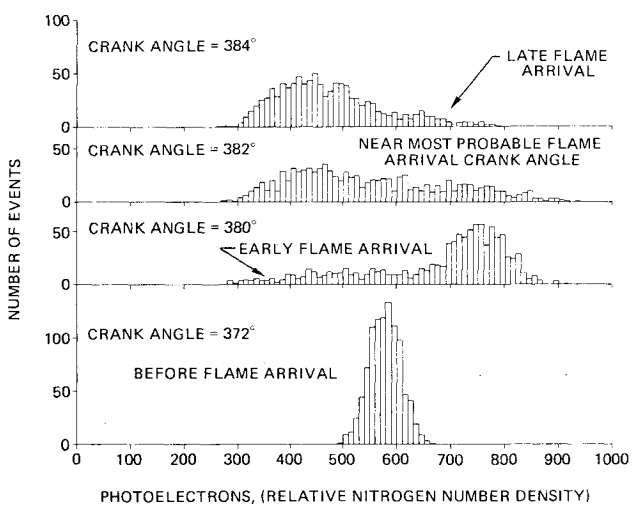

Fig. 4 Histograms of nitrogen number density near time of flame arrival.

probable density value as the mean value of a half distribution and fitting it to a normal curve. The reduction of the apparent fluctuations near the flame arrival crank angle is dramatic. Both curves of Fig. 3 have had the Poisson statistical fluctuations subtracted using Eq. (2).

The histograms of Fig. 4 represent the number of measurements vs the number of photoelectrons at crank

angles near flame arrival in the scattering volume. The bin width is ten photoelectrons and the total number of events is 1000 for each histogram. The normal shape of the histogram at 372 deg is typical of those from 300-372 and 390-420 deg. At 380 deg, early arrival of the flame causes the long tail in the distribution below the most probable density. Similarly, the distortion of the distribution to the higher density values (more photoelectrons) at 384 deg is due to late flame arrivals. This explanation of the effects of cyclic variation on the distribution justifies the attempt to separate them from the real density fluctuations.

The 382-deg histogram appears to be only slightly later than the most probable time of flame arrival. The broad, nearly constant distribution indicates that the flame front is larger than the scattering volume, i.e., thicker than 0.5 mm. This conclusion is supported by bimodal distributions at similar flame arrival times when using scattering volumes of 3-5 mm linear dimensions.

It should be noted that signal-to-noise ratios were of the order of 30:1, even when the flame was in the scattering volume. It is tempting to say the increase in fluctuations immediately behind the flame front is flame-induced turbulence; however, fast fluorescence, which the present Raman system does not discriminate against, may contribute to the signal level. Work in progress should eliminate this concern.

Acknowledgment

This work was supported by the Dept. of Energy and the Motor Vehicle Manufacturers Association.

References

[1] Setchell, R. E., "Raman Spectroscopy Measurements Within a Internal Combustion Engine," 18th Annual Rocky Mountain Spectroscopy Conference, University of Denver, Aug. 1976.

[2] Johnston, S. C., Robinson, C. W., Rorke, W. S., Smith, J. R., and Witze, P. O., "Applications of Laser Diagnostics to an Injected Engine," SAE Paper 790092, Detroit, Mich., Feb. 1979.

[3] Setchell, R. E., "Local Turbulence Properties in Flames From Time-Averaged Raman Spectroscopy Measurements," AIAA Paper 79-0087, New Orleans, La., Jan. 1979.

[4] Tomlinsen, R. G., Damon, E. K., and Buscher, H. T., "The Breakdown of Noble and Atmospheric Gases by Ruby and Neodymium Laser Pulses," *Physics of Quantum Electronics Conference Proceedings 1965*, pp. 520-526.

J80-023
NA
20001
20017

Simple Analytical Modeling of Supersonic Flow around Blunt Axisymmetric Bodies

D.R. Philpott*
The Hatfield Polytechnic, Hatfield, Herts, United Kingdom

Introduction

ALTHOUGH a number of calculation schemes are available for the supersonic blunt body problem, those methods which attempt to solve the complete inviscid equations of motion are too cumbersome for initial design studies, while simplified flow models fail to model important features such as the influence of initial blunting on afterbody pressure.

Pugh and Ward[1] attempted to model this feature by supposing that the layer of slow moving air, or entropy layer, near the body surface, which has been influenced by its passage through the near normal shock wave close to the axis of symmetry, acts like a boundary layer in providing an effective displacement surface which modifies the physical profile of the body. In the present work the same flow model is retained although the entropy layer thickness is defined more precisely and considerable differences are introduced into the calculation scheme. The proposed method thus predicts inviscid wave drag, excluding skin friction and base drag, and is likely to be suitable for initial configuration parameter studies in which economy of computation is important.

Presented as Paper 78-1356 at the AIAA Atmospheric Flight Mechanics Conference, Palo Alto, Calif., Aug. 7-9, 1978; submitted Aug. 17, 1978; revision received July 25, 1979.

Copyright © 1978 by D.R. Philpott. Published by the American Institute of Aeronautics and Astronautics, Inc., with permission.
Index categories: Supersonic and Hypersonic Flow; Aerodynamics.
*Senior Lecturer, School of Engineering.

Derivation of Drag from Shock Wave Profiles

Pugh and Ward[1] determine the wave drag of the body via Oswatitsch's theorem[2] by integrating the entropy flux cross the bow shock wave. Thus only a knowledge of the shock wave geometry is required. For the calculation the shock wave is divided into three zones (Fig. 1). Zone I is the region immediately adjacent to the axis of symmetry and is generated by the initial blunting on the body. Zone II is generated by the afterbody, and it is assumed that the flow is locally nearly conical in this region. Zone III is the far flowfield in which the shock decays to a Mach wave.

Zone I

Pugh and Ward[1] point out that frequently the problem of investigating an afterbody configuration for a particular initial blunting (e.g., spherical) arises, and in their work, as in the present method, an empirical shock wave profile is assumed in this region. However, in order to make the method more readily adaptable to different initial bluntings, an alternative simple prediction method based on Kaattaari's work[3] is currently being investigated for this zone.

Zone II

In zone II the local flow is approximated to a conical flow with a characteristic line running to b at the shock (Fig. 1) from an effective surface at δ^*. In Ref. 1 the displacement thickness of the entropy layer $o\delta^*$ is derived for a parallel afterbody, and the result scaled to account for local density changes in the nonparallel case. It is, however, possible to derive the thickness directly for the nonparallel case as follows: since the mass flow crossing the actual shock Ab and the corresponding conical shock wave ab (Fig. 1) must be equal, and taking dc along the line os

$$\int_0^b 2\pi\rho|y|u\cdot \mathrm{d}c = \int_{\delta^*}^b 2\pi\rho_c|y|u_c\cdot \mathrm{d}c \tag{1}$$

where subscript c refers to the approximate conical flow. This may be rearranged to give the mass flow in the entropy layer

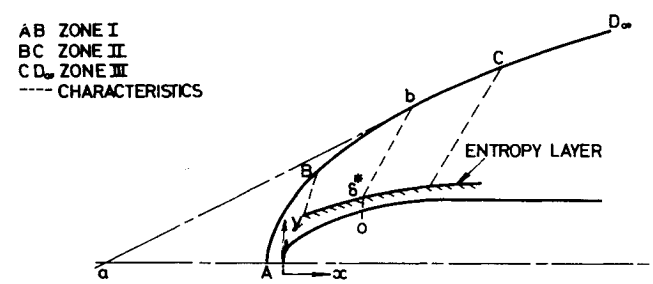

Fig. 1 Shock wave zones.